ACS OMEGA

Open Access

http://pubs.acs.org/journal/acsodf

Article

Assessment of Solubility Behavior of a Copolymer in Supercritical CO_2 and Organic Solvents: Neural Network Prediction and Statistical Analysis

Divya Baskaran, Uma Sankar Behera, and Hun-Soo Byun*

Cite This: *ACS Omega* 2024, 9, 40941−40955

Read Online

ACCESS | Metrics & More | Article Recommendations | Supporting Information

ABSTRACT: In the industrial sector, understanding the behavior of block copolymers in supercritical solvents is crucial. While qualitative agreement with polymer solubility curves has been evaluated using complex theoretical models in many cases, quantitative predictions remain challenging. This study aimed to create a rapid and accurate artificial neural network (ANN) model to predict the lower critical solubility and upper critical solubility space of an atypical block copolymer, poly(styrene-*co*-octafluoropentyl methacrylate) (PSOM), in different supercritical solvent systems over a wide range of temperatures (51.75−182.05 °C) and high pressure (3.28−200.86 MPa). The experimental data set used in this study included one copolymer, five supercritical solvents, one cosolvent, and one initiator. It consisted of seven unique copolymer−solvent combinations (252 cloud point pressures) used to predict the model quantitatively and qualitatively. To predict the PSOM−solvent interactions, the study considered two different input systems: a six-variable system, a five-variable system, and one target output. Initially, we used a three-layer feed-forward neural network to select the best learning algorithm (Levenberg−Marquardt) from 14 different algorithms, considering one sample PSOM−solvent system. Then, the network topology was optimized by varying hidden neuron numbers from 2 to 80 for all seven PSOM−solvent combination systems. The predicted cloud point pressures were in excellent agreement with the experimental cloud point pressures, confirming the model's accuracy. It is clear from the results of a minimum mean square error ($\leq 1.90 \times 10^{-27}$) and maximum linear regression R^2 (≥ 0.99) during training, validation, and testing of all the data sets. Further, the ANN model accuracy was tested by statistical analysis, confirming the model's ability to accurately capture the miscibility regions of polymers, enabling efficient processing of various polymer materials. This data-driven approach facilitates the prediction of coexistence curves for other polymers and complex macromolecular systems.

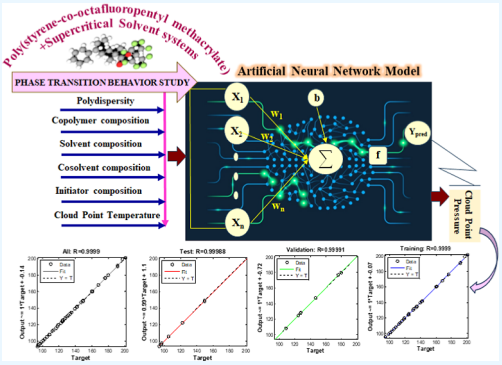

1. INTRODUCTION

Block copolymers have gained significant interest in recent decades due to their unique microphase characteristics, including thermal properties, elasticity, chemical resistance, and tensile strength.[1,2] They find applications in various fields, such as automotive compounds, sports goods, hose tubing, cosmetics, optical coatings, drug delivery, molecular semiconductors, high-density magnetic storage materials, and self-polishing paint applications.[3−5] Examples of different copolymers include Styrene-acrylonitrile copolymer,[6] Styrene-butylene-styrene,[7] nylon-6,6,[8] ethylene chlorotrifluoroethylene,[9] polypropylene random copolymer,[10] etc. A block copolymer's macromolecule consists of different blocks of two or three structured monomers, and it has a reactivity ratio of greater than one.[11] Unlike homopolymers, phase separation is observed at a microscopic level with a better statistical distribution of comonomers, which are chemically linked. The linkage creates classical and complex morphologies in block copolymers, including spheres, cylinders, lamellae, gyroid, and perforated lamellae.[12] To develop solubility interactions with polar solvents and meet the requirements of future technologies, understanding the phase behavior of block copolymers in various conditions such as composition, temperature, and pressure is essential for industrial applications such as the synthesis, processing, self-assembly, and purification of polymeric materials.

The Flory and Huggins lattice model was previously used to capture the thermodynamics of polymer solutions, but it only applies to certain polymer−solvent combinations and has hidden assumptions.[13,14] Later, equation of state,[15,16] active coefficient model,[17−19] and quantity structure−property relationship models[20,21] were developed, but predicting phase behavior remained challenging due to the need to solve

Received: July 4, 2024
Revised: September 8, 2024
Accepted: September 11, 2024
Published: September 19, 2024

multiple complex equations and understand the properties of pure components. Some authors have attempted to quantitatively predict the polymer solubility space for any polymer−solvent pair.[22−25] Supercritical solvents such as water, ionic liquids, and carbon dioxide (CO_2) are particularly useful for predicting polymer phase behavior because of their adjustable features of viscosity, diffusivity, heat capacity, and solubility.[26,27] In some cases, cosolvents, complexing agents, and inverse micelles can be added to the supercritical solvent to improve the solubility limitations of the compounds mentioned above.[28] The miscible-immiscible boundary (cloud point), bubble point, and dew point behavior are part of the phase behavior study and can be identified in the supercritical system.[29] Predicting the coexistence behavior of copolymers and solvents depends on factors such as the properties of the polymer composition, polymer weight-average molecular weight (M_w), polydispersity (PDI), solvent composition, solvent concentration, and processing state variables such as cloud point temperature and cloud point pressure.[30,31] Ethier et al.[31] revealed that the phase behavior may be shifted from upper critical solubility (UCS) to lower critical solubility (LCS) because of increasing polymer molecular weight or reducing pressure. During shifting, UCS reached a higher temperature, and LCS reached a lower temperature, which decreases the area of miscibility percentage.

The separation of thermodynamic phases in binary copolymer solutions depends on both entropic factors (related to polymer size) and enthalpic factors (to monomer−solvent interaction).[32] Researchers have identified common phase behavior for polymer−solvent systems in the literature such as UCS, LCS, isopleths, and closed-loop solubility. Some researchers have studied the phase behavior of different copolymers in supercritical solvents that exhibit UCS and LCS behaviors.[33−35] In some cases, it is necessary to develop a parametrization model to predict the behavior of each polymer binary solution system instead of relying solely on liquid−liquid equilibrium (LLE) experimental data. There are still discrepancies between standard and experimental data, indicating a need for complementary data-driven approaches to predict the LLE data for polymer phase behavior.

Over the past few decades, there has been a growing interest in using machine learning (ML) to speed up the design of various systems in different fields and address their shortcomings.[36−38] Artificial Intelligence neural networks (AI-ANN) are widely used to model and predict linear and nonlinear systems due to their high learning capacity, predictive ability, good performance, nonlinearity, and insensitivity to data noise.[39−41] AI-ANN is a complete black box model and can handle multiple input and output variables, making it a better predictor than conventional empirical models, even when limited information is fed to the system.[42] The learning algorithm plays a crucial role in supervising regression and is responsible for fast and accurate prediction. Interestingly, AI helps to explore data through decision-making, using active learning or experimentation, when the data set is typically scarce. To ensure a reliable model, the quality of the data set and the input and output parameters must be appropriately decided. The use of AI-ANN in polymer science,[43,44] mechanical properties,[45] thermal conductivity,[46] and glass transition temperature[47,48] is rapidly increasing. Ethier et al.[49] used cloud point data (3263 data sets curated from CRC Handbook of LLE data of polymer solutions) to train a deep neural network and Gaussian process regression model to predict UCS and LCS curves. They retrieved the polymer and solvent feature descriptors from the available Hansen solubility parameter (HSP) and topological "fingerprints" and concluded that the ML was used to estimate the HSP even for unknown polymers.

Ethier et al.[31] have curated a data set of 6524 cloud point data points from the CRC Handbook of LLE data of 21 polymers/copolymers and 61 solvents. They tested this data set using two regression models, gradient-boosted decision trees, and ANN, with different descriptors like molecular descriptors, Morgan fingerprints, and HSPs. The goal of their study was to predict the phase behavior of polymer−solvent systems using artificial neural networks (ANNs) and available input and output variables. To investigate the framework of data-driven prediction of LLE data using ANN models, we proposed to predict cloud point pressure using the studied solubility data on binary solutions of block copolymer in various supercritical solvents. We selected a novel poly(styrene-*co*-octafluoropentyl methacrylate) (PSOM) block copolymer in the current study (synthesized by our group; data not shown) due to its biocompatibility and the related block copolymeric materials applied in the field of biomedical, textiles, packaging, and membrane synthesis. As far as we know, there are no such reports published for predicting the phase behavior of complex block copolymer−solvent systems in this direction. This is the first study to predict the LLE data of PSOM in polar and nonpolar solvents using AI-ANN with the help of a learning algorithm.

This proposed study aims to appraise the potency of neural network prediction of the coexistence space data for the block copolymer of PSOM−different supercritical solvent systems. The cloud point pressure data were predicted by seven different systems that contain one polymer and various polar and nonpolar supercritical solvents. Fourteen different back-propagation learning algorithms were tested on the training data, and after screening, the ANN architecture was optimized by varying the neuron number in the three-layer feed-forward network. The attainment of the ANN prediction was checked by correlating the experimental and predicted cloud point pressures, and the prediction accuracy was further tested by statistical analysis. This framework can be extended to different polymers and solvent systems for predicting the LLE data.

2. MATERIALS AND METHODS

2.1. Data Acquisition. The phase transition behavior of a copolymer−solvent system was studied to curate the LLE data set. Our research group recently developed a novel block copolymer of PSOM using dispersion polymerization in a supercritical CO_2 reactor at high pressure.[22] To examine the phase equilibria behavior of PSOM with different solvents, experiments were conducted in a supercritical system with 1-butene (BT), propylene (PP), dimethyl ether (DE), chlorodifluoromethane (CM), BT + tetramethyl orthosilicate (BTTM), DE + tetramethyl orthosilicate (DETM), and carbon dioxide + tetramethyl orthosilicate (CTM). The copolymer synthesis methodology and reactor setup for phase liquid equilibria for a different copolymer [poly(pentyl acrylate-*co*-methyl methacrylate)] were reported in detail by Byun.[33]

The high-pressure reactor setup consists of three sections: a variable volume view cell, a high-pressure pump generator, and a data acquisition system. The working volume and pressure of the cell are 28 cm^3 and 300 MPa, respectively, with an ID of

https://doi.org/10.1021/acsomega.4c06212
ACS Omega 2024, 9, 40941−40955

1.59 cm and an OD of 6.4 cm, used to measure the phase behavior. A rotating piston of about 2.54 cm in size is connected to the high-pressure pump generator where the pressurized water shifts the piston inside the cell. The Heise gauge and digital multimeter thermometer are used to record the pressure and temperature of the mixture of the cell. The solution phase transition behavior was identified through a sapphire window located above the cell. The data acquisition section is interconnected with the borescope camera, which is utilized to visualize the phase transition behavior of the systems. A video monitor is employed for real-time monitoring, where cloud points are identified at different operating conditions.

An initial level of purging was performed in an empty cell several times with the help of nitrogen and supercritical solvents to remove residual foreign contaminants. An appropriate amount of copolymer, solvent, and cosolvent was introduced into the reactor cell by using pressure bombs. The copolymer−solvent-cosolvent sample inside the reactor cell was subjected to compression until a one-phase reaction was achieved. To ensure thermal stability, maintain the equilibrium condition under a pressurized environment for 30 min. Later, the pressure was slowly reduced until the solution system exhibited cloudiness. The observed opalescence point in the solution was termed as a cloud point. The cloud point pressure measurements were performed three times at each temperature condition and the average measurements for copolymer in different supercritical solvent systems.

The data set consists of 252 cloud points, including one copolymer called PSOM, five supercritical solvents (BT, PP, DE, CM, and CO_2), one cosolvent (TM), and one initiator [2,2-azobis(isobutyronitrile)] (AN). There are seven unique copolymer−solvent systems in the data set. The study used the PSOM copolymer with different M_w of 49.5, 42.4, 33.8, 26.8, 24.1 kDa and corresponding PDI values 2.9, 1.94, 2.25, 2.94, and 2.07, respectively. Further, AN composition varied from 1, 2, to 4% by mass. The copolymer compositions varied to 2.7, 2.8, 3, 3.1, 3.2, and 3.4% by mass. The study investigated the phase behavior of the copolymer across different compositions of PSOM and different supercritical polar and nonpolar solvents at temperatures ranging from 51.75 to 182.05 °C and high pressure ranging from 3.28 to 200.86 MPa in the supercritical system. The LLE solubility curves of UCS and LCS behavior were observed for seven different copolymer binary solvent systems used for the data-driven process. These measurements were reproduced at least twice, with a precision of within ±0.28 MPa and ±0.20 °C. The physical properties of supercritical solvents such as chemical formula, M_w, critical pressure (T_p), critical temperature (T_c), dipole moment (μ), acentric factor (ω), and polarizability (α) are displayed in Table S1.

The data set for the solubility curve includes different components of polymer, solvent, and state variables. Input parameters include PDI, copolymer composition (mass %), solvent composition (mass %), cosolvent composition (mass %), initiator composition (mass %), and cloud point temperature (°C). The target parameter for developing the ANN model is the cloud point pressure (MPa). Out of the seven-variable systems, four systems considered the five-variable system and three systems considered the six-variable system. The name of the system is based on the input variables taken for data-driven processing. Table 1 displays the input and target components of the polymer, solvent, and state variables involved in ANN modeling. The data were collected at different compositions of copolymer and solvent and corresponding to different values of cloud point temperature. Ethier et al. predicted the LLE data using ML for different polymer−solvent systems where the minimum number of cloud points used is 7 and the maximum of 991.[49] Although the amount of available data for every system is excellent, for developing the ANN model for LLE prediction in the current study, data collection accuracy is based on the reproducibility of phase transition measurements, and uncertainties are ±0.28 and 0.40 MPa for cloud point pressure and ±0.20 °C for cloud point temperature, respectively.

Table 1. Input and Target Components of Copolymer, Solvent, and State Variables Involved in ANN Modeling

	input parameters	
	five-variable system	six-variable system
IP1	PDI	PDI
IP2	copolymer composition (mass %)	copolymer composition (mass %)
IP3	solvent composition (mass %)	solvent composition (mass %)
IP4	initiator composition (mass %)	co-solvent composition (mass %)
IP5	cloud point temperature (°C)	initiator composition (mass %)
IP6		cloud point temperature (°C)
	target parameter	
TP1	cloud point pressure (Mpa)	cloud point pressure (Mpa)

2.2. ANN Modeling. The black-box models are preferred over white-box models, and ANN is one such black-box model because it does not require any preliminary knowledge of structure, properties, and relationship between the input and target variables. In this study, a three-layer neural network was used, and it comprises an input layer, one hidden layer, and an output layer. Each of these layers consists of many neurons, and these are connected to those in the adjacent layers via weights (w) and biases (b). The selection of a learning algorithm and optimization of neuron topology is very crucial in developing the ANN model.[50,51] The neuron number of the input layer and output layer is based on the integer of input and target variables, respectively. The network has a transfer function of the sigmoid (tansig) in hidden neurons and is linear in output neurons (purelin), suitable for this regression task. Figure 1 shows the schematic representation of the ANN architecture showing the input, hidden, and target variables of phase equilibria behavior study for the six-variable (Figure 1a) and five-variable systems (Figure 1b).

The selection of the hidden layer is based on the process complexity, and it is determined by a trial-and-error procedure and is calculated by using eq 1.[42]

$$O_j = \mathrm{F}(I_j) \tag{1}$$

where O_j, I_j, and F are the input of ith neuron, the output of ith neuron, and the transfer function, respectively. There are two functions such as weighted summation and transformation functions used in the hidden layer that predict the target value. The input of each neuron (I_j) is calculated by eq 2 concerning outputs from the previous layers (O_j), weights connecting the ith neuron to the jth neuron (w_{ij}) and bias of the jth neuron (b_j).[40]

$$I_j = \sum iw_{ij}y_i + b_j \tag{2}$$

The activation function used in the hidden layer is a sigmoid function, which is represented by eq 3

https://doi.org/10.1021/acsomega.4c06212
ACS Omega 2024, 9, 40941−40955

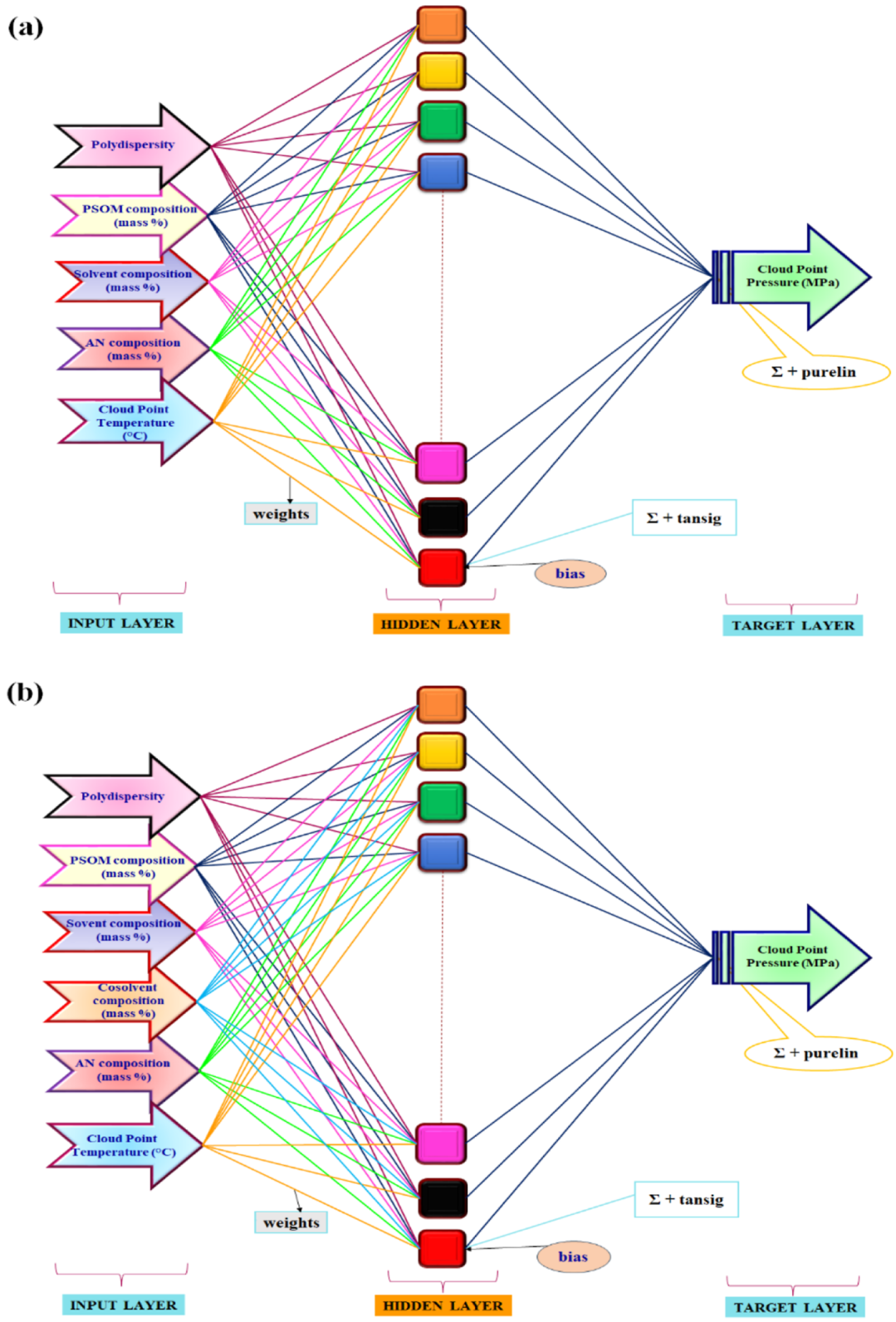

Figure 1. Schematic representation of the ANN architecture showing the input, hidden, and target variables of phase equilibria behavior study for (a) five-variable and (b) six-variable systems.

$$f(I_j) = \frac{1}{1 + e^{-I_j}} \quad (3)$$

2.3. Optimization of Training Algorithms and ANN Topology. The experimental data for the cloud point were randomly divided into three parts, using the dividerand algorithm: 70% for training, 15% for validation, and 15% for testing. This division helps in rigorously training the data sets. The training set is used to train and adjust the network based on its error value. The validation data set is used to benchmark the network's generalization, and the testing data set is used to

https://doi.org/10.1021/acsomega.4c06212
ACS Omega 2024, 9, 40941−40955

evaluate the network's independent performance during and after training. To optimize the weights and biases of the network, learning algorithms need to be screened. In this investigation, the ANN model was tested with 14 back-propagation (BP) learning algorithms, such as BFGS Quasi-Newton (Trainbfg), bayesian regulation (Trainbr), conjugate gradient with Beale-Powell restarts (Traincgb), conjugate gradient BP with Fletcher-Reeves restarts (Traincgf), conjugate gradient with Polak-Ribiere restarts (Traincgp), gradient descent (Traingd), gradient descent with momentum (Traingdm), gradient descent with adaptive learning rate (Traingda), gradient descent with momentum and adaptive learning rate (Traingdx), Levenberg−Marquardt (Trainlm), one step secant (Trainoss), random weight/bias rule (Trainr), Rprop-Resilient (Trainrp), and scaled conjugate gradient (Trainscg). Each training algorithm has individual and peculiar merits and limitations. The study used the Learngdm adaptive function. Initially, the number of neurons in the hidden layer was fixed at 10 to select the best BP learning algorithm.

Table 2 shows the internal network training parameters used for choosing the best BP algorithm and ANN architecture for the phase behavior equilibrium. The minimum mean squared error (MSE) plays a pivotal role in the selection and advised training of the network to reach a local minimum MSE and maximum correlation coefficient (R^2) between the targeted and predicted data. Following the screening of the BP algorithm, the ANN architecture was optimized by varying the hidden layer neurons from 2 to 80 and all other parameters are constant. The factual ANN architecture is reached after iterating the process several times until the MSE reaches a satisfactory level. The best validation was performed by reducing the epochs to minimum error. The best network topology depends upon the integer of hidden layers, neuron number of the hidden layer (N_H), learning rate (η), epoch size (E_c), momentum term (α), BP algorithm adjustment parameter (μ), training cycle, and transfer function.

Table 2. Internal Network Training Parameters for Choosing the Best BP Algorithm and ANN Architecture

parameters	best value
total number of epochs (E_c)	1000
number of neurons in the input layer fixed for two different systems	5 and 6
the range of number of neurons used in the hidden layer (N_H) for topology optimization	2−80
number of neurons in the target layer	1
learning rate (η)	0.001
transfer function used in the hidden and target layers	tansig and purelin
error tolerance	0.001
data division (random)	dividerand (70:15:15)
adaptive function	Learngdm
network type	feed-forward BP
training algorithm	14 BP algorithms (screen: Levenberg−Marquardt)
performance	MSE
adjustment parameter (μ)	0.005
momentum value (α)	0.9

2.4. Model Training of Cloud Points and Sensitivity Analysis. The block copolymer PSOM is soluble in different supercritical solvents such as PSOM−BT, PSOM−PP, PSOM−DE, PSOM−CM, PSOM−BTTM, PSOM−DETM, and PSOM−CTM systems. To determine the solubility behavior of PSOM in these solvents, the predicted cloud point pressure parameter is used. The training of the ANN has been carried out by using 252 cloud point data sets for different solvents, i.e., UCS and LCS. Among the seven different copolymer−solvent systems, the PSOM−BT system has been selected for finding the best learning algorithm. Since the number of data sets of the PSOM−BT system is much higher (56 data sets) than the other systems, it has been taken as a model to be involved in the algorithm screening process at fixed hidden layer neurons (10). Then, the optimum topology has been identified for all the copolymer−solvent systems by training seven data sets separately by varying neurons from 2 to 80. The performance of all seven copolymer−solvent phase liquid equilibria was evaluated by increasing the hidden layer neuron number. The topology of all seven systems has been identified by training until reaching the minimum error with R^2. The best learning algorithm and topology can predict the cloud point pressures with ±0.28 MPa uncertainty values observed in the MSE values for PSOM in various solvents. Finally, the parity plots developed between the observed benchmark values and the corresponding predicted values. The plots have been used to evaluate the significance of the model fitting and coexistence behavior of the copolymer−different supercritical solvent systems.

The performance of the ANN model was estimated for its prediction accuracy using different statistical parameters such as mean error (ME), MSE, root MSE (RMSE), standard error of prediction (SEP %), average absolute relative deviation (AARD %), bias factor (B_f), and Accuracy factor (A_f). In addition, a linear regression analysis (R^2) between the experimental target values and the network-predicted values was evaluated. Thus, the closeness of model values to the experimental ones was determined using the equations below (4−11).[39]

$$\mathrm{ME} = \frac{\sum_{i=1}^{n} (T_{i,\mathrm{exp}} - T_{i,\mathrm{pre}})}{n} \tag{4}$$

$$\mathrm{MSE} = \frac{\sum_{i=1}^{n} (T_{i,\mathrm{exp}} - T_{i,\mathrm{pre}})^2}{n} \tag{5}$$

$$\mathrm{RMSE} = \sqrt{\frac{\sum_{i=1}^{n} (T_{i,\mathrm{exp}} - T_{i,\mathrm{pre}})^2}{n}} \tag{6}$$

$$\mathrm{SEP}\ (\%) = \frac{\mathrm{RMSE}}{\overline{T}_{i,\mathrm{exp}}} \times 100 \tag{7}$$

$$\mathrm{AARD}\ (\%) \frac{\sum_{i=1}^{n} \left(\left| \frac{T_{i,\mathrm{exp}} - T_{i,\mathrm{pre}}}{T_{i,\mathrm{exp}}} \right| \right)}{n} \times 100 \tag{8}$$

$$B_F = 10^{[\sum_{i=1}^{n} \log(T_{i,\mathrm{pre}}/T_{i,\mathrm{exp}})/n]} \tag{9}$$

$$A_F = 10^{[\sum_{i=1}^{n} \log|T_{i,\mathrm{pre}}/T_{i,\mathrm{exp}}|/n]} \tag{10}$$

$$R^2 = 1 - \frac{\sum_{i=1}^{n} (T_{i,\mathrm{exp}} - T_{i,\mathrm{pre}})^2}{\sum_{i=1}^{n} (T_{i,\mathrm{exp}} - \overline{T}_{i,\mathrm{exp}})^2} \tag{11}$$

https://doi.org/10.1021/acsomega.4c06212
ACS Omega 2024, 9, 40941−40955

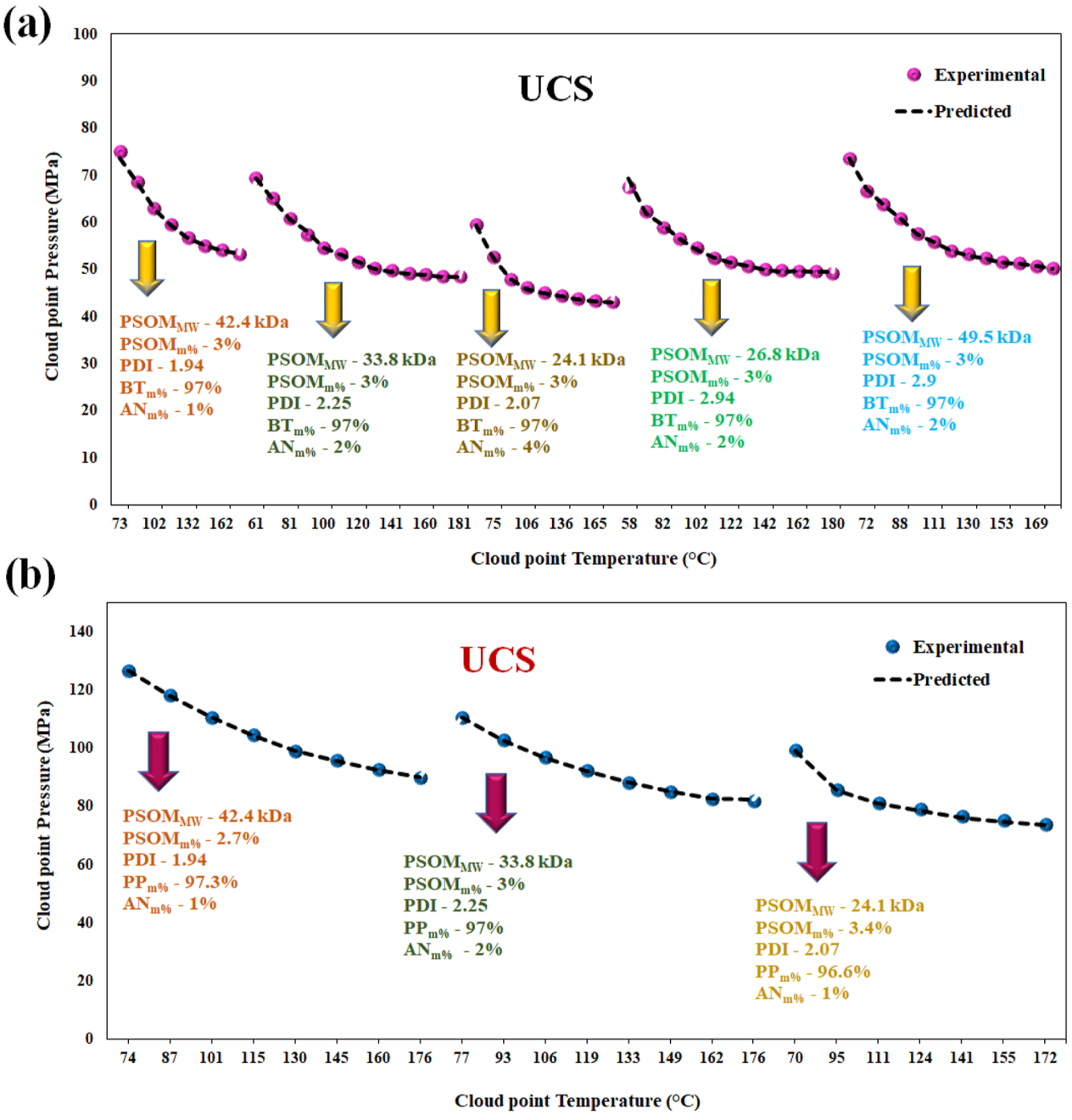

Figure 2. Cloud point profile of phase transition behavior of (a) PSOM−BT and (b) PSOM−PP systems.

where $T_{i,\mathrm{exp}}$, $T_{i,\mathrm{pre}}$, and $\overline{T}_{i,\mathrm{exp}}$ are the experimental, predicted, and mean experimental outputs, respectively, and n is the number of experiments.

2.5. Software Utilization. ANN modeling codes were generated, and the entire training, validation, and testing was performed by using the shareware version of the ML-ANN software of MATLAB (Version 7.11.0.584, R2016b) utilizing Neural network Toolbox, The Math Works Inc., USA.

3. RESULTS AND DISCUSSION

3.1. Experimental Phase Transition Behavior of Copolymer Binary Solvent Systems. The data used in this study on copolymer-supercritical solvent phase behavior consist of 4 data sets with five variables and 3 data sets with six variables. These data sets were obtained from our recent research work, but the data are not shown. The cloud point from the phase behavior experiment is used to examine the range of copolymer-supercritical solvent solubility space over a wide range of temperatures from 51.75 to 182.05 °C and pressures from 3.28 to 200.86 MPa. The experimental cloud point profile of the copolymer−solvent system shows the predictive performance of an UCS and LCS of PSOM in different supercritical polar and nonpolar solvents such as BT, PP, DE, CM, BTTM, DETM, and CTM.

Figures 2−4 demonstrate the cloud point pressure as a function of cloud point temperature, which exhibited an upper critical solution behavior for PSOM-BT (Figure 2a), PSOM−PP (Figure 2b), and PSOM-CM (Figure 3b) systems, whereas lower critical solution behavior was observed for PSOM-DE (Figure 3a), PSOM-BTTM (Figure 4a), and PSOM-DETM

https://doi.org/10.1021/acsomega.4c06212
ACS Omega 2024, 9, 40941−40955

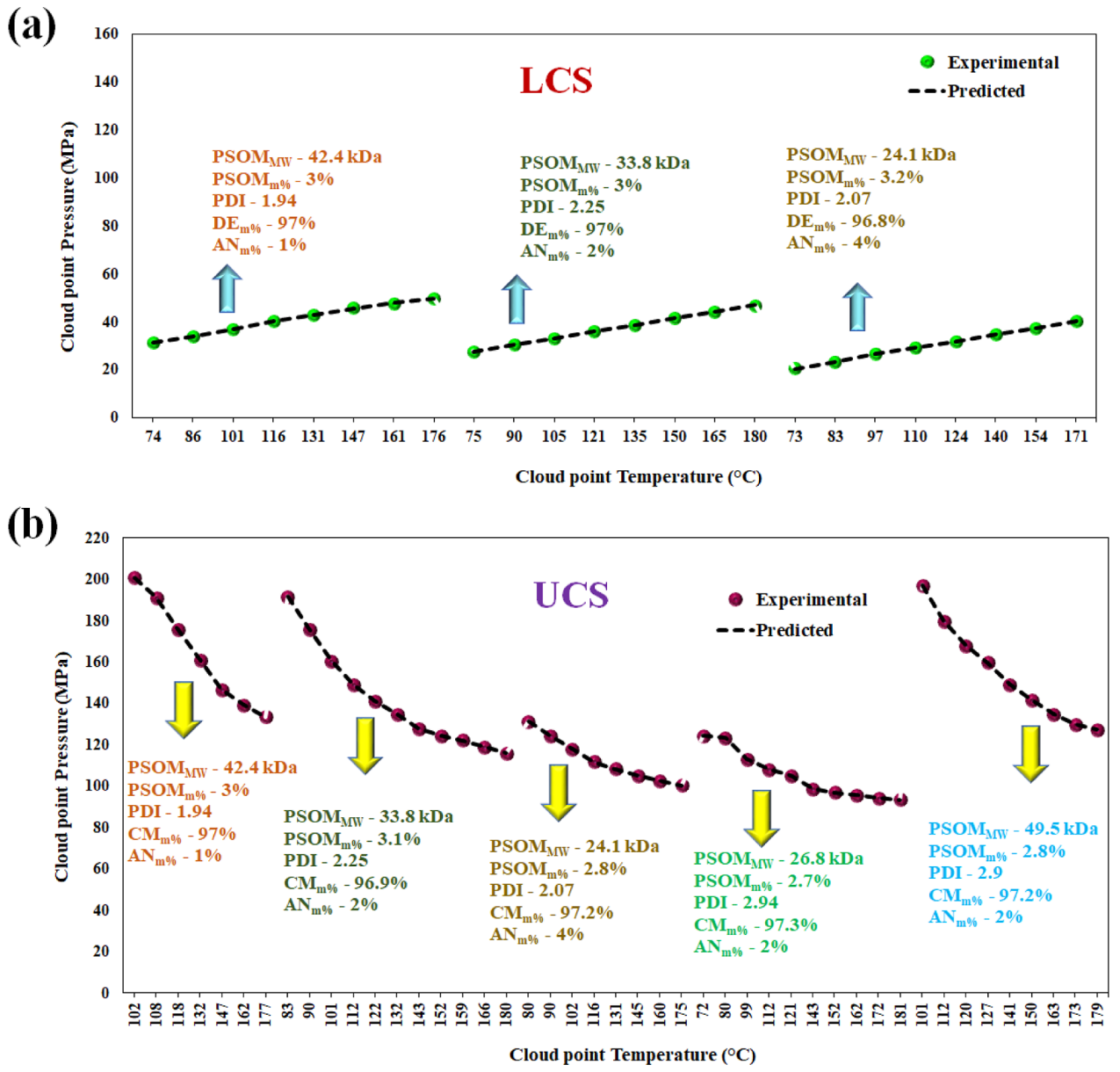

Figure 3. Cloud point profile of phase transition behavior of (a) PSOM−DE and (b) PSOM−CM systems.

(Figure 4b). Interestingly, the phase transition pressure curve of PSOM in BTTM and CTM shifted from UPS to LCS behavior when the temperature was increased (Figure 4c). Therefore, the two types of binodal curves obtained in the above-mentioned systems show that the solubility of copolymer PSOM decreased asymmetrically for both polar, nonpolar, and combinations of solvents, and reducing the pressure plays a role.

The cloud point pressure of the solubility space varies depending on the solvents and cosolvent systems used. Among the UCS types, the block copolymer PSOM achieved the cloud point at supercritical pressures of 197.24 and 198.79 MPa in CM and CTM solvent systems, respectively. The PSOM-carbon dioxide + tetramethyl orthosilicate system reached the LCS behavior through the maximum cloud point pressure of 70.86 MPa. The composition and type of solvent and cosolvent have a significant effect on the solubility space of block copolymer PSOM, but they do not have any significant effects on the other properties of the polymer, solvent, cosolvent, and initiator. However, the coexistence space shifted from UCS to LCS behavior (Figure 4c) due to decreasing the solvent (CO_2) composition from 53.4 to 27.8 mass % and increasing the cosolvent (TM) composition from 44 to 68.9 mass % at a constant loading of the initiator. This lowest solubility curve is achieved for the CO_2 system due to limited molecular interactions because of the nonpolar solvent. The pressure of cloud points or coexistence points observed in all systems was found to decrease with increasing temperature. Similar trends were observed in recently published works for different polymer-supercritical solvent systems.[26,52,53] The binodal curve data sets are used for the ANN modeling to predict the accuracy of the observations.

3.2. Training Algorithm Optimization. ANN is a proposed method for predicting the coexistence behavior of seven different binary solutions of the PSOM block copolymer. The system uses either five or six variables with between five and six inputs and one target variable. A neural network is fed these data to model the performance of LLE behavior. To

https://doi.org/10.1021/acsomega.4c06212
ACS Omega 2024, 9, 40941−40955

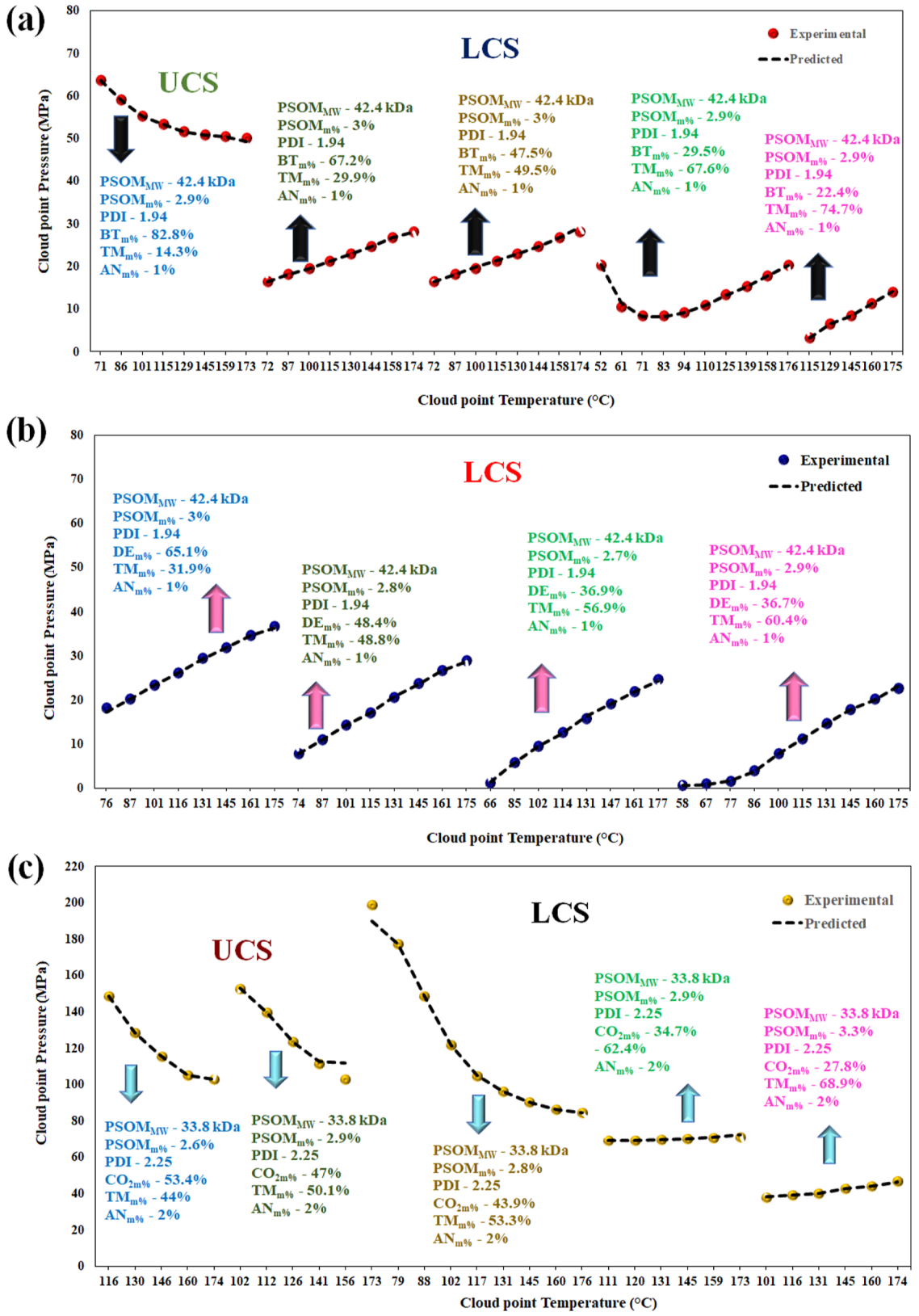

Figure 4. Cloud point profile of phase transition behavior of (a) PSOM−BTTM, (b) PSOM−DETM, and (c) PSOM−CTM systems.

randomly divide the experimental data, the dividerand algorithm was used. A total of 176 data points were used for training, 38 for validation, and 38 for testing the ANN model. Various authors have used a percentage of 70, 15, and 15 for training, validation, and testing, respectively, across different data sets and have found that it yields the best network and more accurate training of the model.[54,55] Similarly, training data were used to train the neural network by assigning small weights to connections between nodes in a random manner. The weights were reinitiated by reverting input ranges until a

https://doi.org/10.1021/acsomega.4c06212
ACS Omega 2024, 9, 40941−40955

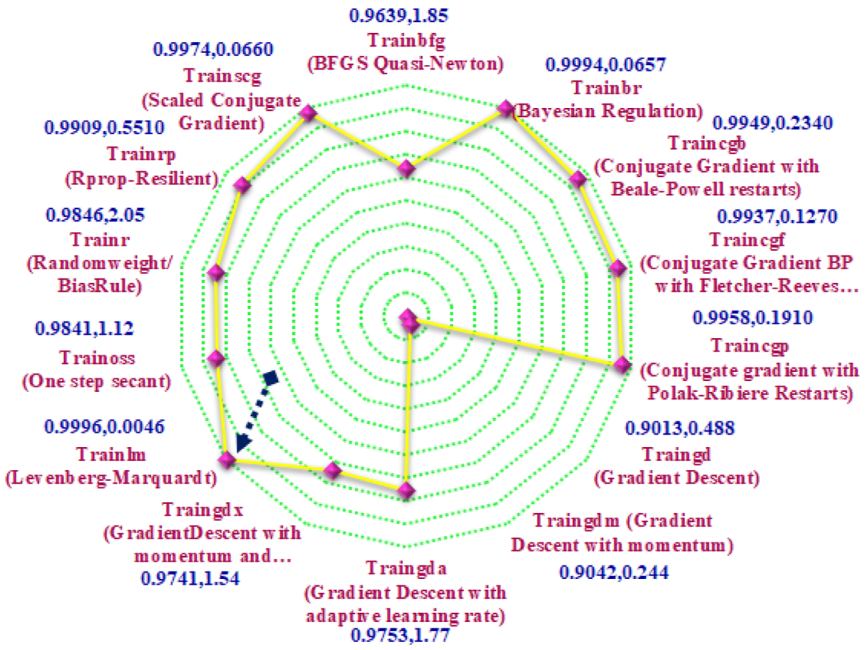

Figure 5. Comparison profile of different BP training algorithms based on the performance of R^2 and MSE for the copolymer PSOM−BT system.

minimum MSE was achieved between the observed and predicted values of the target cloud point pressure, which was carried out in the validation process. The accuracy of the predicted LLE data was then appraised using the test data set.

The copolymer PSOM−BT supercritical solvent system was used as a sample data set to determine the best learning algorithm among seven different binary polymer solution systems. Fourteen BP learning algorithms were employed to train the ANN model data set, including Trainbfg, Trainbr, Traincgb, Traincgf, Traincgp, Traingd, Traingdm, Traingda, Traingdx, Trainlm, Trainoss, Trainr, Trainrp, and Trainscg. The algorithm with the minimum MSE and a higher correlation coefficient was selected as the best. All of these learning algorithms applied the three-layer feedforward BP network with a transfer function of Tansig hidden neurons and purelin target neurons. During the screening process, the neuron number in the hidden layer was kept constant at 10 (N_H) to avoid any noise. The BP training algorithm parameters (E_c, η, μ, α, and error tolerance) were set to default values (Table 2), with values fixed at 1000, 0.001, 0.005, 0.9, and 0.001, respectively. These parameter values were chosen based on previous ANN modeling experience in the field of biochemical engineering,[50] and they all play a crucial role in network convergence and attaining local minimum error. In the copolymer PSOM−BT supercritical system, five neurons were applied to the input layer and one to the target layer.

Table S2 displays a comparison of 14 different BP training algorithms, using values of MSE, R^2, and iteration numbers, for predicting cloud point pressure. Figure 5 illustrates a comparison profile based on the performance of MSE and R^2 received from the algorithm selection process in the copolymer PSOM-BT system. The Levenberg−Marquardt BP algorithm achieved the minimum training error value of 0.0046 and a maximum R^2 value of 0.9996, making it the best BP learning algorithm for the ANN modeling of copolymer PSOM-different solvent systems. During optimization, the "trainlm" training function was used to update the weights and bias values, to ensure a close fit between the target of observed and predicted values of the entire network and to minimize the performance (MSE) function. However, the training was stopped once the consecutive iterations and validation MSE started to increase. While trainbr and traincg algorithms approached minimum error (0.0657 and 0.0660) with maximum R^2 (0.9994 and 0.9974), the least error algorithm was chosen for the proposed study. On the other hand, trainbfg (0.9639 and 1.85), traingd (0.9013 and 0.488), traingdm (0.9042 and 0.244), traingda (0.9753 and 1.77), and traingdx (0.9741 and 1.54) BP algorithms had poor performance on the prediction of cloud point pressure. Other studies have also found that the "trainlm" algorithm is the best and fastest learning algorithm for different fields of data sets in ANN modeling.[56−58]

3.3. ANN Topology and Execution. The architecture or neuron topology optimization of an ANN plays a decisive role in the training of the ANN model. The hidden layer neurons are highly sensitive to the neural network, and the neuron number in the hidden layer is an important factor in determining the performance of the model. Insufficient neurons lead to poor performance, while an excessive number of neurons can create turbulence in the prediction. This study used a trial-and-error approach to optimize the internal network parameters (N_H) for copolymer−different supercritical solvent systems. The outperformed BP training algorithm was screened immediately, and the N_H value varied from 2 to 80 during optimization, while other parameters were kept constant for all seven PSOM-supercritical solvent systems to predict the cloud point pressure. The training process was halted once the minimum MSE was achieved. The weight and bias values were generated using the "trainlm" training function until the model output closely matched the target MSE. Two tables (Tables S3 and S4) were used to show the optimization of the ANN architecture via correlation coefficient, MSE, and iteration numbers in five-variable and six-variable copolymer binary solution systems, respectively.

The seven systems had five or six input neurons, including PDI, copolymer composition, solvent composition, initiator

https://doi.org/10.1021/acsomega.4c06212
ACS Omega 2024, 9, 40941−40955

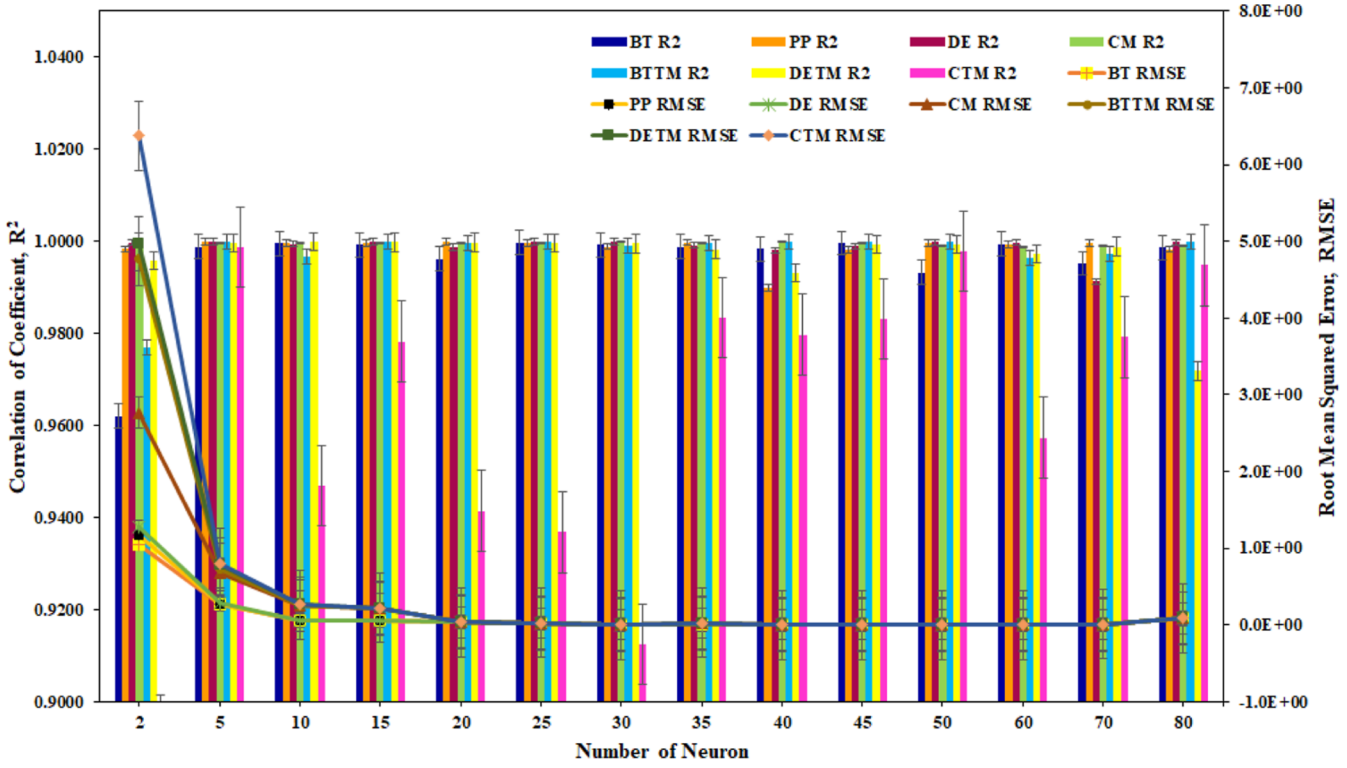

Figure 6. Effect of different neuron numbers on MSE and R^2 values for copolymer−different supercritical solvent systems.

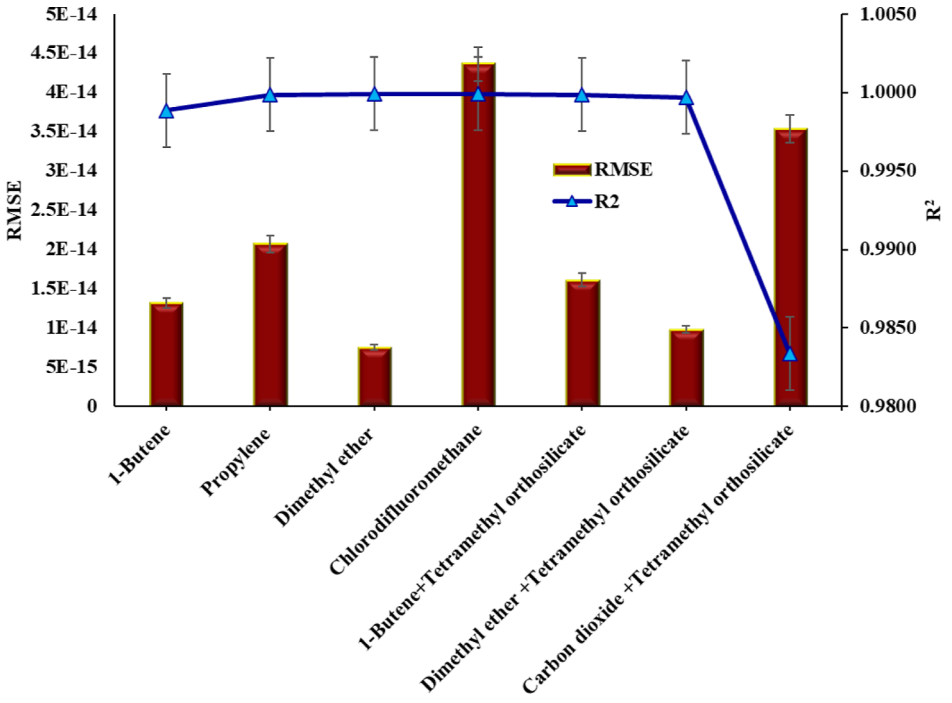

Figure 7. Comparison of performance error and regression correlation coefficient between each solvent's data set using the ANN model.

composition, cosolvent composition, and cloud point temperature, and one output parameter (cloud point pressure) was used for the development of the ANN model. The best neuron number, R^2, MSE, and iteration number were highlighted for all of the systems in Table S3 and S4. The optimum neuron number was found to be 35, 20, 15, 30, 25, 25, and 35 with a minimum MSE value of 1.74×10^{-28}, 4.28×10^{-28}, 5.68×10^{-29}, 1.90×10^{-27}, 2.60×10^{-28}, 9.66×10^{-29} and 1.25×10^{-27} and a maximum R^2 value of 0.9989, 0.9999, 0.9999, 0.9999, 0.9999, 0.9997, and 0.9834 for predicting the cloud point pressure in the PSOM−BT, PSOM−PP, PSOM−DE, PSOM−CM, PSOM−BTTM, PSOM−DETM and PSOM−CTM systems, respectively.

Interestingly, the training was continued and stopped at very few iterations (epochs) between 5 and 6 for all systems (Figures S1 and S2). As a result, the optimized ANN

https://doi.org/10.1021/acsomega.4c06212
ACS Omega 2024, 9, 40941−40955

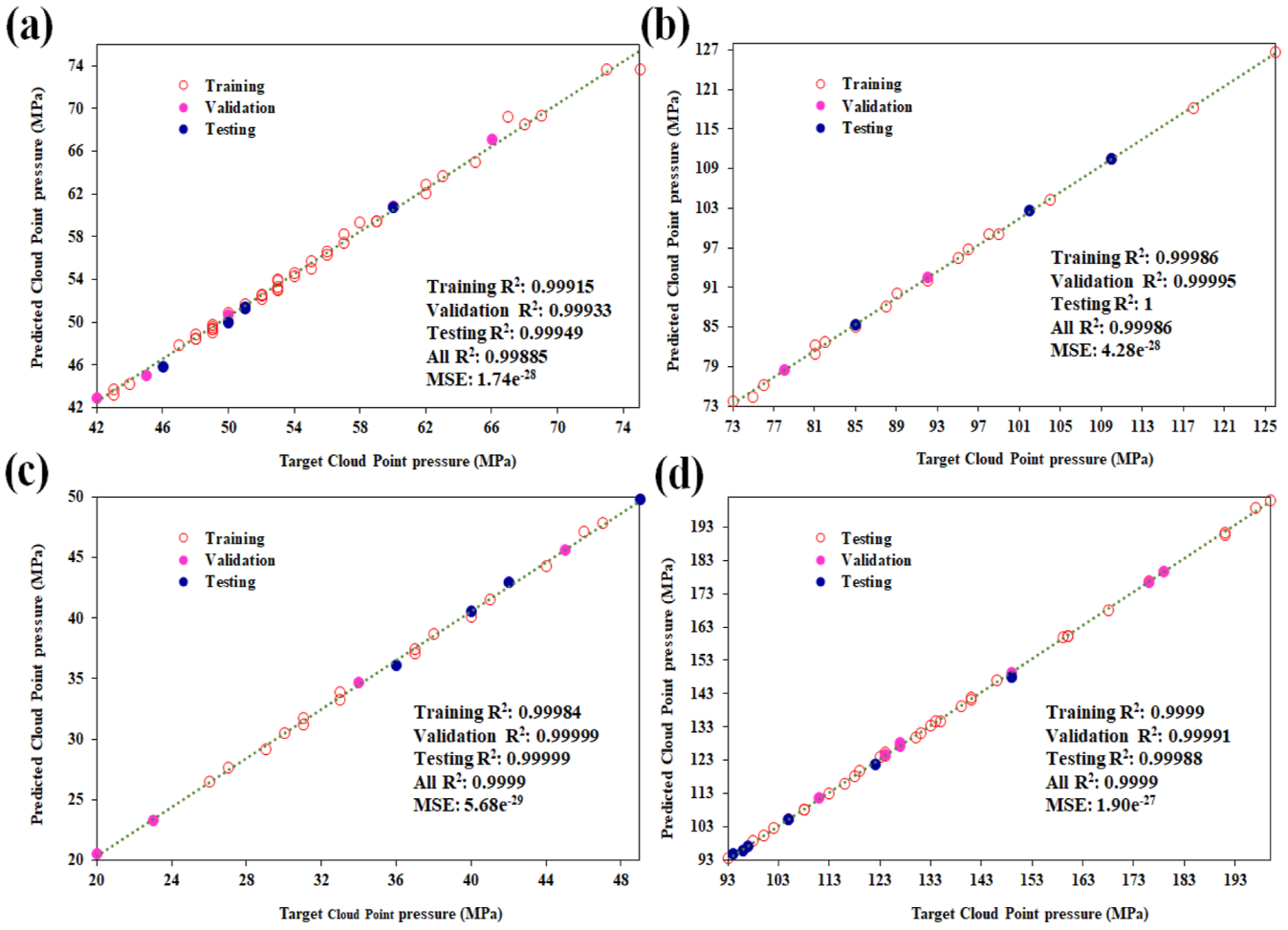

Figure 8. Parity plots showing ANN predicted cloud point pressure plotted against the experimental cloud point pressure for (a) PSOM−BT, (b) PSOM−PP, (c) PSOM−DE, and (d) PSOM−CM systems.

architecture/topology was found to be 5:35:1, 5:20:1, 5:15:1, 5:30:1, 6:25:1, 6:25:1 and 6:35:1 for the copolymer-different solvent systems containing BT, PP, DE, CM, BTTM, DETM, and CTM, respectively. Figure 6 depicts the effect of neuron numbers on the performance of copolymer−solvent systems. Increasing the neuron number after reaching consecutive N_H values improved the performance error, but the RMSE value did not change significantly. On the other hand, the R^2 value showed a sharp decrease. Similar results were reported in other studies.[59,60] Ethier et al. achieved the minimum RMSE with 64 neurons in predicting cloud point temperature with 3263 data sets.[49] In this study, however, less than or equal to 35 neurons were sufficient to obtain outstanding performance in various solvent systems with a maximum of 252 data sets. Therefore, the studied systems have a better ANN architecture.

Furthermore, Figure 7 provides a comparison profile of RMSE and R^2 values for each solvent system's data set performance using the ANN model. Among different supercritical solvent data sets, the DE data set showed the least RMSE (5.68×10^{-29}) and the highest R^2 (0.9999) with copolymer PSOM. However, the CM solvent data set showed a maximum error of 1.90×10^{-27} compared to other solvent systems, even though it achieved a maximum R^2 value like other solvent data sets. Nevertheless, the regression correlation coefficient reached ≥0.9990 for all solvent systems, whereas the PSOM-carbon dioxide + tetramethyl orthosilicate system attained a lower value of 0.98339. Table S5 displays the optimum weights and biases of the ANN architecture related to the "trainlm" algorithm for different phase behavior systems. The weight matrix of w_1 and w_2 belongs to the input and hidden layers, respectively, while b_1 and b_2 are for the input and output layers. The weight magnitude determines the connection strength between the input and hidden layer neurons. The sign of the weight, either − or +, denotes the nature of the correlation between input and hidden layer neurons.[61,62] To predict the experimental target of cloud point pressure, eq 1 is used by reinitializing the w_1, w_2, b_1, and b_2 and reverting input parameters between the network layers.

3.4. Phase Behavior Prediction Potency of ANN.

Figures S3 and S4 show the linear regression analysis between the predicted and experimental cloud point pressures for various phase behavior systems. The linear regression performance of the PSOM−BT, PSOM−PP, PSOM−DE, and PSOM−CM systems are shown in Figure S3 while PSOM−BTTM, PSOM−DETM and PSOM−CTM systems are shown in Figure S4. These figures explain the linear regression analysis between the experimental target (T) and the predicted target (Y) values of the cloud point pressure. The binary solution systems reached a maximum correlation coefficient of ≥0.98032. The parity plots in Figures 8 and 9 demonstrate the linear regression performance and MSE values for all systems. Figure 8 shows the parity plots for five-variable systems, and

https://doi.org/10.1021/acsomega.4c06212
ACS Omega 2024, 9, 40941−40955

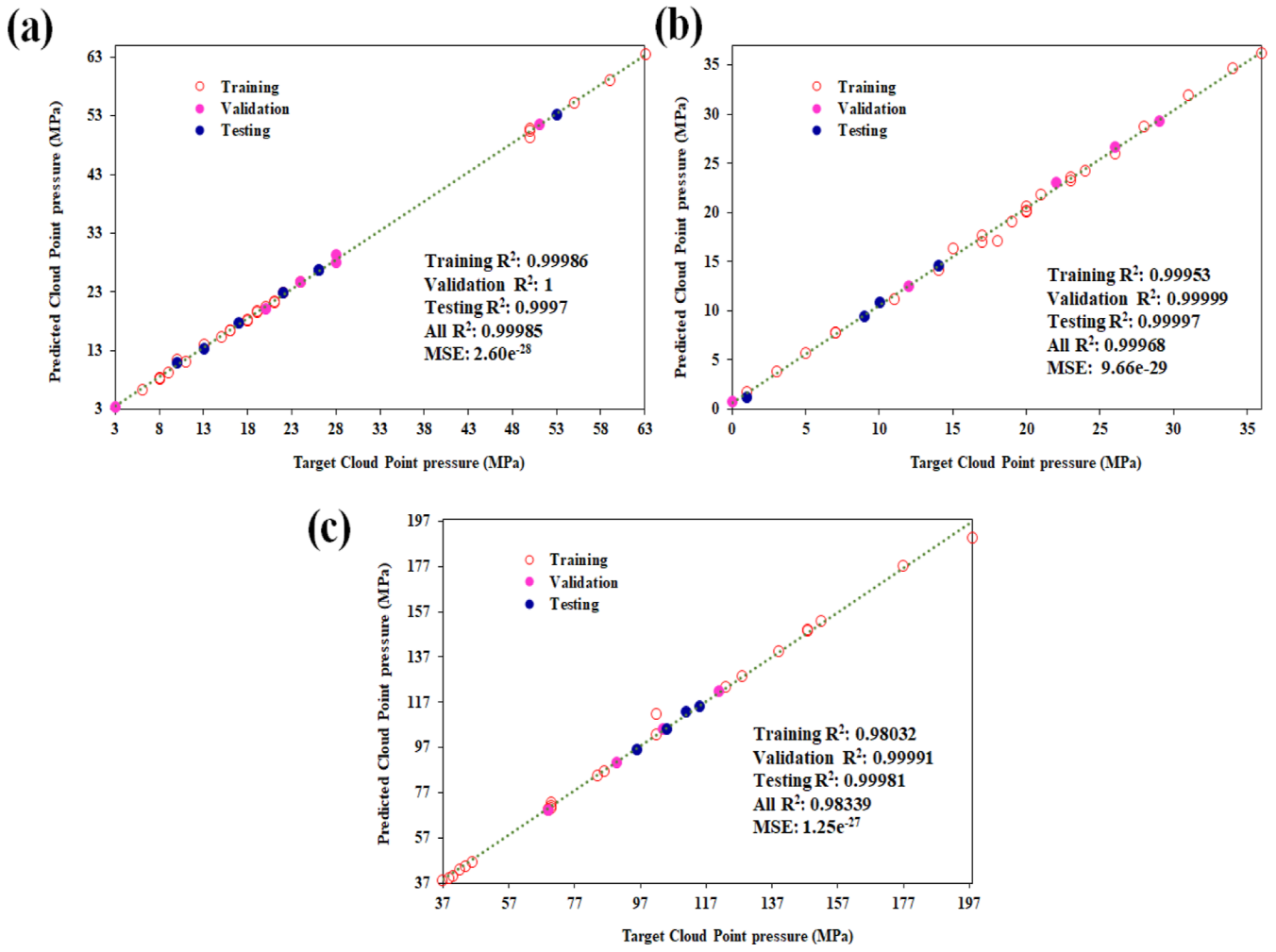

Figure 9. Parity plots showing ANN predicted cloud point pressure plotted against the experimental cloud point pressure for (a) PSOM−BTTM, (b) PSOM−DETM, and (c) PSOM−CTM systems.

Table 3. Statistical Analysis of the Different System Training, Validation, and Testing Data for the ANN Model Accuracy Prediction[a]

	five-variable system				six-variable system		
accuracy parameters	BT	PP	DE	CM	BTTM	DETM	CTM
ME	0.0597	0.0051	0.0087	0.0181	0.0474	0.0428	0.0991
MSE	0.1327	0.0584	0.0130	0.0904	0.0817	0.0638	0.1630
RMSE	0.3643	0.2416	0.1140	0.3006	0.2859	0.2526	0.4038
SEP (%)	0.6673	0.2590	0.3140	0.2233	1.1528	1.4774	0.4159
AARD (%)	0.4745	0.1919	0.1725	0.1583	0.7439	1.7148	0.2383
bias factor, B_f	1.0016	0.9998	1.0000	1.0002	1.0028	0.9951	1.0013
accuracy factor, A_f	1.0016	0.9998	1.0000	1.0002	1.0028	0.9951	1.0013
regression correlation coefficient, R^2	0.9996	0.9997	0.9998	0.9998	0.9997	0.9993	0.9973
slope	1	1	1	1	1	1	0.93
Y-axis intercept	−0.18	−0.4	−0.14	−0.14	0.12	0.023	6.5

[a]BT: 1-butene; PP: propylene; DE: dimethyl ether; CM: chlorodifluoromethane; BTTM: BT + tetramethyl orthosilicate; DETM: DE + tetramethyl orthosilicate; CTM: carbon dioxide + tetramethyl orthosilicate.

Figure 9 shows those for six-variable systems. In both figures, the solid line at 45° indicates an excellent match between the predicted and observed phase liquid equilibrium curves.

Collectively, the linear regression performance of training, validation, testing, and all with MSE value for all systems are reported in the parity plots. The different systems of PSOM−BT (Figure 8a), PSOM−PP (Figure 8b), PSOM−DE (Figure 8c), PSOM−CM (Figure 8d), PSOM−BTTM (Figure 9a), PSOM−DETM (Figure 9b), and PSOM−CTM (Figure 9c) achieved the training R^2 value of 0.99915, 0.99986, 0.99984, 0.9999, 0.99986, 0.99953, and 0.98032; validation R^2 value of 0.99933, 0.99995, 0.99999, 0.99991, 1, 0.99999, and 0.99991; testing R^2 value of 0.99949, 1, 0.99999, 0.99988, 0.9997, 99997, and 0.99981; overall R^2 value of 0.99885, 0.99986,

https://doi.org/10.1021/acsomega.4c06212
ACS Omega 2024, 9, 40941−40955

0.9999, 0.9999, 0.99985, 0.99968, and 0.98339, respectively. For all the data sets, the value of R^2 is within an acceptable level and corroborates an upstanding agreement with the experimental target data.

Hence, the ANN-predicted cloud point pressure data set was taken and plotted with the function of cloud point temperature for different systems for PSOM−BT (Figure 2a), PSOM−PP (Figure 2b), PSOM−DE (Figure 3a), PSOM−CM (Figure 3b), PSOM−BTTM (Figure 4a), PSOM−DETM (Figure 4b), and PSOM−CTM (Figure 4c). The solubility curves show that the cloud point pressure observation for various systems matches better the ANN predicted values. Among the UCS types, the PSOM-CM system's phase transition behavior has achieved better agreement ($R^2 \geq 0.9999$) than other systems. Similarly, among the LCS type, the PSOM−DE system's phase transition behavior has achieved better agreement ($R^2 \geq 0.9999$) than other systems. However, the PSOM−CTM system's prediction performance ($R^2 \geq 0.98339$) was reduced from other systems due to the type of solvent containing minimal dipole moment compared to other solvents. Therefore, the solubility of the system is much affected by the noise of the data set. Nonetheless, the linear regressions of all UCS and LCS cloud point pressures indicated that the ANN model is reliable in predicting cloud point pressures, securing good performance. Many studies have reported that $R^2 \geq 0.98339$ is a better linear regression and had good agreement with the predicted and experimental target data set.[39]

3.5. Statistical Analysis of the Model. Furthermore, the accuracy of the ANN predictions and the degree of fitness were computed by using equations from 4 to 11 and the results are tabulated in Table 3. In this table, the accuracy parameters of the five-variable system and six-variable system training, validation, and testing data for the ANN model are laid out. The ANN model accuracy was analyzed in the form of statistical parameters such as ME, MSE, RMSE, SEP %, AARD %, B_f, and A_f for predicting cloud point pressures of different copolymer binary solvent systems. The observed values of the accuracy parameters of ME (0.0597, 0.0051, 0.0087, 0.0181, 0.0474, 0.0428 and 0.0991), MSE (0.1327, 0.0584, 0.0130, 0.0904, 0.0817, 0.0638 and 0.1630), RMSE (0.3643, 0.2416, 0.1140, 0.3006, 0.2859, 0.2526, 0.4038), SEP % (0.6673, 0.2590, 0.3140, 0.2233, 1.1528, 1.4774, 0.4159), and AARD % (0.4745, 0.1919, 0.1725, 0.1583, 0.7439, 1.7148, 0.2383) for the systems of PSOM−BT, PSOM−PP, PSOM−DE, PSOM−CM, PSOM−BTTM, PSOM−DETM, and PSOM−CTM, respectively. The parameters mentioned above have values that are lower than those expected for all systems. This suggests that the ANN model is accurate in predicting the phase transition behavior of the block copolymer in supercritical solvents. Additionally, the values of the B_f and A_f factors are close to unity, indicating that the modeled network is valid for predicting the solubility space of PSOM in different polar and nonpolar solvent solution systems.

During the linear regression analysis, the R^2 value mentioned in Table 3 is close to the values displayed in Figures 8 and 9. Furthermore, the slope value is close to unity, and the y-intercept is almost negligible for all phase transitional behavior systems (Figures S2 and S3). Therefore, all computed values are within reasonable limits and confirm that the experimental target data fit well with the ANN-predicted data. Consequently, ANN can accurately predict and model the cloud point pressures and define the actual phase behavior with LCS and UCS solubility curves of the block copolymer PSOM in different supercritical solvent systems. Although the application of ANN models in diverse fields of study has been reported elsewhere,[63−67] there are no reports on the phase transition behavior of block copolymer-supercritical solution systems. Therefore, this study is the first to predict the cloud point pressures using ANN and can help nurture research in ANN themes for assessing the performance of the solubility space of polymer−solvent systems.

4. CONCLUSIONS AND OUTLOOK

An ANN model has been developed to predict the phase transition curve of block copolymer accurately and quickly in different polar and nonpolar supercritical solvents. This model can handle 3 six-variable and 4 five-variable systems to predict the UCS and LCS behavior. The ANN architecture was optimized using the best training algorithm (trainlm), and the optimum topology was determined by the coexistence curves with minimum RMSE maximum R^2. For the seven studied systems (PSOM−BT, PSOM−PP, PSOM−DE, PSOM−CM, PSOM−BTTM, PSOM−DETM, and PSOM−CTM), the optimized ANN architecture was found to be 5:35:1, 5:20:1, 5:15:1, 5:30:1, 6:25:1, 6:25:1, and 6:35:1, respectively. The ANN model's accuracy was evaluated using statistical parameters ME, MSE, RMSE, SEP %, AARD %, B_f, A_f, and R^2. The linear regression R^2 values for training, validation, testing, and overall were all within an acceptable range, confirming that the ANN model's predicted cloud point pressures are in good agreement with the experimental cloud point pressures and are valid for the study. This model can predict smoother polymer solubility curves, and its accuracy and benefits for active ML have been demonstrated. The model's competence to capture regions of miscibility accurately for polymers will license the well-planned polymer material processing. Additionally, this study emphasizes the importance of exploring the proficiency of training models to compute the phase behavior of other macromolecular architectures.

■ ASSOCIATED CONTENT

Supporting Information

The Supporting Information is available free of charge at https://pubs.acs.org/doi/10.1021/acsomega.4c06212.

Physical properties of supercritical solvents; comparison of different BP algorithm prediction results; optimization results of PSOM−BT, PSOM−PP, PSOM−DE, and PSOM−CM; optimization results of PSOM−BTTM, PSOM−DETM, and PSOM−CTM; weights and biases of the optimized ANN models for all systems; effect of training state results of PSOM−BT, PSOM−PP, PSOM−DE, and PSOM−CM; effect of training state results of PSOM−BTTM, PSOM−DETM, and PSOM−CTM; linear regression results of PSOM−BT, PSOM−PP, PSOM−DE, and PSOM−CM; and linear regression results of PSOM−BTTM, PSOM−DETM, and PSOM−CTM (PDF)

■ AUTHOR INFORMATION

Corresponding Author

Hun-Soo Byun − *Department of Chemical and Biomolecular Engineering, Chonnam National University, Yeosu, Jeonnam 59626, S. Korea;* orcid.org/0000-0003-2356-8515;

https://doi.org/10.1021/acsomega.4c06212
ACS Omega 2024, 9, 40941−40955

Phone: +82-61-659-7296; Email: hsbyun@jnu.ac.kr; Fax: +82-61-659-7299

Authors

Divya Baskaran − *Department of Chemical and Biomolecular Engineering, Chonnam National University, Yeosu, Jeonnam 59626, S. Korea*

Uma Sankar Behera − *Department of Chemical and Biomolecular Engineering, Chonnam National University, Yeosu, Jeonnam 59626, S. Korea;* orcid.org/0000-0002-1388-0401

Complete contact information is available at: https://pubs.acs.org/10.1021/acsomega.4c06212

Notes

The authors declare no competing financial interest.

■ ACKNOWLEDGMENTS

This work was supported by the National Research Foundation of Korea (NRF) grant funded by the Korean government (MSIT) (no. 2021R1A2C2006888).

■ REFERENCES

(1) Baeza, G. P. Recent advances on the structure−properties relationship of multiblock copolymers. *J. Polym. Sci.* **2021**, *59*, 2405−2433.
(2) Steube, M.; Johann, T.; Barent, R. D.; Müller, A. H.; Frey, H. Rational design of tapered multiblock copolymers for thermoplastic elastomers. *Prog. Polym. Sci.* **2022**, *124* (No), 101488.
(3) Kim, H. J.; Jeong, C.; Oh, A.; Seo, Y. S.; Jeon, H.; Eom, Y. Elevated volatile organic compound emissions from coated thermoplastic polyester elastomer in automotive interior parts: Importance of plastic swelling. *J. Hazard. Mater.* **2024**, *461* (No), 132614.
(4) Choudhury, S.; Ray, S. K. Sorption thermodynamics and coupling effect for pervaporative dehydration of acetone through nanoclay and iron nanoparticle-filled copolymer membranes. *Korean J. Chem. Eng.* **2022**, *39*, 529−547.
(5) Huang, C.; Zhu, Y.; Man, X. Block copolymer thin films. *Phys. Rep.* **2021**, *932*, 1−36.
(6) Asteasuain, M.; Pintos, E.; Fortunatti, C.; Brandolin, A.; Sarmoria, C. Modeling of the activators regenerated by electron transfer copolymerization of styrene-acrylonitrile with prediction of the bivariate molecular weight distribution-copolymer composition distribution using parallel computing and probability generating functions. *Ind. Eng. Chem. Res.* **2023**, *62*, 145−157.
(7) Zhao, C.; Chen, X.; Chen, X. A morphological study of dynamically vulcanized styrene-ethylene-butylene-styrene/styrene-butylene-styrene/methylvinylsilicon rubber thermoplastic elastomer. *Polymers* **2022**, *14* (9), 1654.
(8) Rashed, K.; Kafi, A.; Simons, R.; Bateman, S. Fused filament fabrication of nylon 6/66 copolymer: Parametric study comparing full factorial and Taguchi design of experiments. *Rapid Prototyp. J.* **2022**, *28*, 1111−1128.
(9) Zhang, X.; Chen, F.; Su, Z.; Xie, T. Effect of radiation-induced cross-linking on thermal aging properties of ethylene-tetrafluoroethylene for aircraft cable materials. *Materials* **2021**, *14* (2), 257.
(10) Rabbani, F. A.; Yasin, S.; Iqbal, T.; Farooq, U. Experimental study of mechanical properties of polypropylene random copolymer and rice-husk-based biocomposite by using nanoindentation. *Materials* **2022**, *15* (5), 1956.
(11) Xia, X.; Gao, T.; Li, F.; Suzuki, R.; Isono, T.; Satoh, T. Multidimensional control of repeating unit/sequence/topology for one-step synthesis of block polymers from monomer mixtures. *J. Am. Chem. Soc.* **2022**, *144*, 17905−17915.
(12) Xu, Z.; Li, W. Control the self-assembly of block copolymers by tailoring the packing frustration. *Chin. J. Chem.* **2022**, *40*, 1083−1090.
(13) Schmid, F. Understanding and modeling polymers: The challenge of multiple scales. *ACS Polym. Au* **2023**, *3*, 28−58.
(14) Chapman, W. G.; Fouad, W. A. Beyond Flory-Huggins: Activity coefficients from Perturbation theory for polar, polarizable, and associating solvents to polymers. *Ind. Eng. Chem. Res.* **2022**, *61*, 17644−17664.
(15) Ghoderao, P. N.; Lee, C. W.; Byun, H. S. Phase behavior investigation of the vinyl toluene and poly (vinyl toluene)+ co-solvents in supercritical CO_2. *J. Ind. Eng. Chem.* **2023**, *121*, 92−99.
(16) Dhamodharan, D.; Lee, C. W.; Byun, H. S. High-pressure phase equilibrium of the binary systems CO_2+ 355-TMHA and CO_2+ 335-TMCHMA. *New J. Chem.* **2023**, *47*, 4043−4051.
(17) Kontogeorgis, G. M.; Saraiva, A.; Fredenslund, A.; Tassios, D. P. Prediction of liquid-liquid equilibrium for binary polymer solutions with simple activity coefficient models. *Ind. Eng. Chem. Res.* **1995**, *34*, 1823−1834.
(18) Wu, Y. T.; Zhu, Z. Q.; Lin, D. Q.; Mei, L. H. A modified NRTL equation for the calculation of phase equilibrium of polymer solutions. *Fluid Phase Equilib.* **1996**, *121*, 125−139.
(19) Kuo, Y. C.; Hsu, C. C.; Lin, S. T. Prediction of phase behaviors of polymer−solvent mixtures from the COSMO-SAC activity coefficient model. *Ind. Eng. Chem. Res.* **2013**, *52*, 13505−13515.
(20) Amamoto, Y. Data-driven approaches for structure-property relationships in polymer science for prediction and understanding. *Polym. J.* **2022**, *54*, 957−967.
(21) Park, J.; Staiger, A.; Mecking, S.; Winey, K. I. Structure−Property Relationships in Single-Ion Conducting Multiblock Copolymers: A Phase Diagram and Ionic Conductivities. *Macromolecules* **2021**, *54*, 4269−4279.
(22) Behera, U. S.; Baskaran, D.; Byun, H. S. Phase behavior of the mixtures of 2-and 3-components for poly (styrene-co-octafluoropentyl methacrylate) by dispersion polymerization under co2. *ACS Omega* **2024**, *9*, 11910−11924.
(23) Baskaran, D.; Chinnappan, K.; Manivasagan, R.; Selvaraj, R. Liquid-liquid equilibrium of polymer-inorganic salt aqueous two-phase systems: experimental determination and correlation. *J. Chem. Eng. Data* **2017**, *62*, 738−743.
(24) Rao, W.; Wang, Y.; Han, J.; Wang, L.; Chen, T.; Liu, Y.; Ni, L. Cloud point and liquid−liquid equilibrium behavior of thermosensitive polymer L61 and salt aqueous two-phase system. *J. Phys. Chem. B* **2015**, *119*, 8201−8208.
(25) Li, W.; Zhu, Z. Q.; Li, M. Measurement and calculation of liquid-liquid equilibria of binary aqueous polymer solutions. *J. Chem. Eng.* **2000**, *78*, 179−185.
(26) Baskaran, D.; Park, C. W.; Behera, U. S.; Byun, H. S. Phase equilibria of binary mixtures of 3-chloro-2-hydroxypropyl methacrylate and 2-n-morpholinoethyl methacrylate in supercritical carbon dioxide. *Korean J. Chem. Eng.* **2024**, *41*, 2675−2689.
(27) Behera, U. S.; Prasad, S. K.; Byun, H. S. Experimental validation on the phase separation for the 2-(Diisopropylamino) ethyl methacrylate and Poly [2-(diisopropylamino) ethyl methacrylate] in supercritical CO_2. *J. Mol. Liq.* **2024**, *393*, 123553.
(28) Ghoderao, P. N.; Dhamodharan, D.; Mubarak, S.; Byun, H. S. Phase behavioral study of binary systems for the vinyl benzoate, vinyl pivalate and vinyl octanoate with carbon dioxide at high-pressure. *J. Mol. Liq.* **2022**, *358*, 119131.
(29) Park, M. S.; Baskaran, D.; Byun, H. S. Equilibrium curves and modeling of binary systems for the carbon di-oxide+ benzyl acetoacetate and carbon di-oxide+ benzyl acetate mixtures under high pressure. *Thermochim. Acta* **2024**, *740*, 179832.
(30) Kuperkar, K.; Patel, D.; Atanase, L. I.; Bahadur, P. Amphiphilic block copolymers: their structures, and self-assembly to polymeric micelles and polymersomes as drug delivery vehicles. *Polymers* **2022**, *14*, 4702.
(31) Ethier, J. G.; Casukhela, R. K.; Latimer, J. J.; Jacobsen, M. D.; Rasin, B.; Gupta, M. K.; Baldwin, L. A.; Vaia, R. A. Predicting phase behavior of linear polymers in solution using machine learning. *Macromolecules* **2022**, *55*, 2691−2702.

(32) Ajitha, A. R.; Thomas, S. Introduction: Polymer blends, thermodynamics, miscibility, phase separation, and compatibilization. *Compatibilization of Polymer Blends*; Academic Press: Elsevier, 2020, pp 1−29.
(33) Byun, H. S. Phase separation of two-and three-component solution for the poly (pentyl acrylate-co-methyl methacrylate) + compressed solvents and copolymer preparation by supercritical dispersion polymerization. *J. Ind. Eng. Chem.* **2021**, *99*, 158−171.
(34) Lee, B. S. Miscibility of poly (lactide-co-glycolide) in supercritical fluids. *J. Mol. Liq.* **2023**, *369*, 120853.
(35) Gangapurwala, G.; Vollrath, A.; De San Luis, A.; Schubert, U. S. PLA/PLGA-based drug delivery systems produced with supercritical CO_2-A green future for particle formulation? *Pharmaceutics* **2020**, *12*, 1118.
(36) Alballa, N.; Al-Turaiki, I. Machine learning approaches in COVID-19 diagnosis, mortality, and severity risk prediction: A review. *Inform. Med. Unlocked* **2021**, *24*, 100564.
(37) Çınar, Z. M.; Nuhu, A. A.; Zeeshan, Q.; Korhan, O.; Asmael, M.; Safaei, B. Machine learning in predictive maintenance towards sustainable smart manufacturing in industry 4.0. *Sustainability* **2020**, *12*, 8211.
(38) Cova, T. F.; Pais, A. A. Deep learning for deep chemistry: optimizing the prediction of chemical patterns. *Front. Chem.* **2019**, *7*, 809.
(39) Sinharoy, A.; Baskaran, D.; Pakshirajan, K. Process integration and artificial neural network modeling of biological sulfate reduction using a carbon monoxide fed gas lift bioreactor. *J. Chem. Eng.* **2020**, *391*, 123518.
(40) Rajamanickam, R.; Baskaran, D. Neural network model for biological waste management systems. In *Current Trends and Advances in Computer-Aided Intelligent Environmental Data Engineering*; Academic Press, Elsevier, 2022; pp 393−415.
(41) Negi, B. B.; Aliveli, M.; Behera, S. K.; Das, R.; Sinharoy, A.; Rene, E. R.; Pakshirajan, K. Predictive modelling and optimization of an airlift bioreactor for selenite removal from wastewater using artificial neural networks and particle swarm optimization. *Environ. Res.* **2023**, *219*, 115073.
(42) Baskaran, D.; Rajamanickam, R.; Pakshirajan, K. Experimental studies and neural network modeling of the removal of trichloroethylene vapor in a biofilter. *J. Environ. Manage.* **2019**, *250*, 109385.
(43) Gormley, A. J.; Webb, M. A. Machine learning in combinatorial polymer chemistry. *Nat. Rev. Mater.* **2021**, *6*, 642−644.
(44) Kumar, J. N.; Li, Q.; Jun, Y. Challenges and opportunities of polymer design with machine learning and high throughput experimentation. *MRS Commun.* **2019**, *9*, 537−544.
(45) Jordan, B.; Gorji, M. B.; Mohr, D. Neural network model describing the temperature-and rate-dependent stress-strain response of polypropylene. *Int. J. Plast.* **2020**, *135*, 102811.
(46) Wu, S.; Kondo, Y.; Kakimoto, M. A.; Yang, B.; Yamada, H.; Kuwajima, I.; Lambard, G.; Hongo, K.; Xu, Y.; Shiomi, J.; et al. Machine-learning-assisted discovery of polymers with high thermal conductivity using a molecular design algorithm. *npj Comput. Mater.* **2019**, *5*, 66.
(47) Tao, L.; Varshney, V.; Li, Y. Benchmarking machine learning models for polymer informatics: an example of glass transition temperature. *J. Chem. Inf. Model.* **2021**, *61*, 5395−5413.
(48) Alcobaça, E.; Mastelini, S. M.; Botari, T.; Pimentel, B. A.; Cassar, D. R.; de Carvalho, A. C. P. d. L. F.; Zanotto, E. D. Explainable machine learning algorithms for predicting glass transition temperatures. *Acta Mater.* **2020**, *188*, 92−100.
(49) Ethier, J. G.; Casukhela, R. K.; Latimer, J. J.; Jacobsen, M. D.; Shantz, A. B.; Vaia, R. A. Deep learning of binary solution phase behavior of polystyrene. *ACS Macro Lett.* **2021**, *10*, 749−754.
(50) Paul, T.; Aggarwal, A.; Behera, S. K.; Meher, S. K.; Gupta, S.; Baskaran, D.; Rene, E. R.; Pakshirajan, K.; Pugazhenthi, G. Neuro-fuzzy modelling of a continuous stirred tank bioreactor with ceramic membrane technology for treating petroleum refinery effluent: a case study from Assam, India. *Bioprocess Biosyst. Eng.* **2024**, *47*, 91−103.
(51) Maksum, Y.; Amirli, A.; Amangeldi, A.; Inkarbekov, M.; Ding, Y.; Romagnoli, A.; Rustamov, S.; Akhmetov, B. Computational acceleration of topology optimization using parallel computing and machine learning methods−analysis of research trends. *J. Ind. Inf. Integr.* **2022**, *28*, 100352.
(52) Choo, Y. S.; Yeo, W. H.; Byun, H. S. Phase equilibria and cloud-point behavior for the poly (2-phenylethyl methacrylate) in supercritical CO_2 with monomers as co-solvent. *J. CO2 Util.* **2019**, *31*, 215−225.
(53) Ghoderao, P. N.; Kim, J.; Byun, H. S. Binary solution behavior for the trimethoxyphenylsilane and trimethylphenylsilane under co_2 as supercritical fluid. *Ind. Eng. Chem. Res.* **2023**, *62*, 21428−21436.
(54) Sada, S. O.; Ikpeseni, S. C. Evaluation of ANN and ANFIS modeling ability in the prediction of AISI 1050 steel machining performance. *Heliyon* **2021**, *7*, No. e06136.
(55) Ianni, J. D.; Soans, R. E.; Sankarapandian, S.; Chamarthi, R. V.; Ayyagari, D.; Olsen, T. G.; Bonham, M. J.; Stavish, C. C.; Motaparthi, K.; Cockerell, C. J.; et al. Tailored for real-world: a whole slide image classification system validated on uncurated multi-site data emulating the prospective pathology workload. *Sci. Rep.* **2020**, *10*, 3217.
(56) Özdoğan, H.; Üncü, Y. A.; Şekerci, M.; Kaplan, A. Estimations for (n, α) reaction cross sections at around 14.5 MeV using Levenberg-Marquardt algorithm-based artificial neural network. *Appl. Radiat. Isot.* **2023**, *192*, 110609.
(57) Huang, X.; Cao, H.; Jia, B. Optimization of Levenberg Marquardt Algorithm Applied to Nonlinear Systems. *Processes* **2023**, *11*, 1794.
(58) Bui, X. N.; Muazu, M. A.; Nguyen, H. Optimizing Levenberg−Marquardt backpropagation technique in predicting factor of safety of slopes after two-dimensional OptumG2 analysis. *Eng. Comput.* **2020**, *36*, 941−952.
(59) Liu, Q. F.; Iqbal, M. F.; Yang, J.; Lu, X. Y.; Zhang, P.; Rauf, M. Prediction of chloride diffusivity in concrete using artificial neural network: Modelling and performance evaluation. *Constr. Build. Mater.* **2021**, *268*, 121082.
(60) Rostami, S.; Toghraie, D.; Shabani, B.; Sina, N.; Barnoon, P. Measurement of the thermal conductivity of MWCNT-CuO/water hybrid nanofluid using artificial neural networks (ANNs). *J. Therm. Anal. Calorim.* **2021**, *143*, 1097−1105.
(61) López, M. E.; Rene, E. R.; Boger, Z.; Veiga, M. C.; Kennes, C. Modelling the removal of volatile pollutants under transient conditions in a two-stage bioreactor using artificial neural networks. *J. Hazard. Mater.* **2017**, *324*, 100−109.
(62) Hodassman, S.; Vardi, R.; Tugendhaft, Y.; Goldental, A.; Kanter, I. Efficient dendritic learning as an alternative to synaptic plasticity hypothesis. *Sci. Rep.* **2022**, *12*, 6571.
(63) Baskaran, D.; Sinharoy, A.; Paul, T.; Pakshirajan, K.; Rajamanickam, R. Performance evaluation and neural network modeling of trichloroethylene removal using a continuously operated two-phase partitioning bioreactor. *Environ. Technol. Innov.* **2020**, *17*, 100568.
(64) Raja, S.; Thivaharan, V.; Ramesh, V.; Murty, V. R. Prediction of viscosities of aqueous two-phase systems containing protein by artificial neural network. *J. Chem. Eng. Process Technol.* **2014**, *5*, 3−5.
(65) Armaghani, D. J.; Asteris, P. G. A comparative study of ANN and ANFIS models for the prediction of cement-based mortar materials compressive strength. *Neural Comput. Appl.* **2021**, *33*, 4501−4532.
(66) Chen, Y.; Song, L.; Liu, Y.; Yang, L.; Li, D. A review of the artificial neural network models for water quality prediction. *Appl. Sci.* **2020**, *10*, 5776.
(67) Elbeltagi, E.; Wefki, H. Predicting energy consumption for residential buildings using ANN through parametric modeling. *Energy Rep* **2021**, *7*, 2534−2545.

https://doi.org/10.1021/acsomega.4c06212
ACS Omega 2024, 9, 40941−40955